Article

Current Biology

Evolutionary tuning of an auditory transduction channel

Graphical abstract

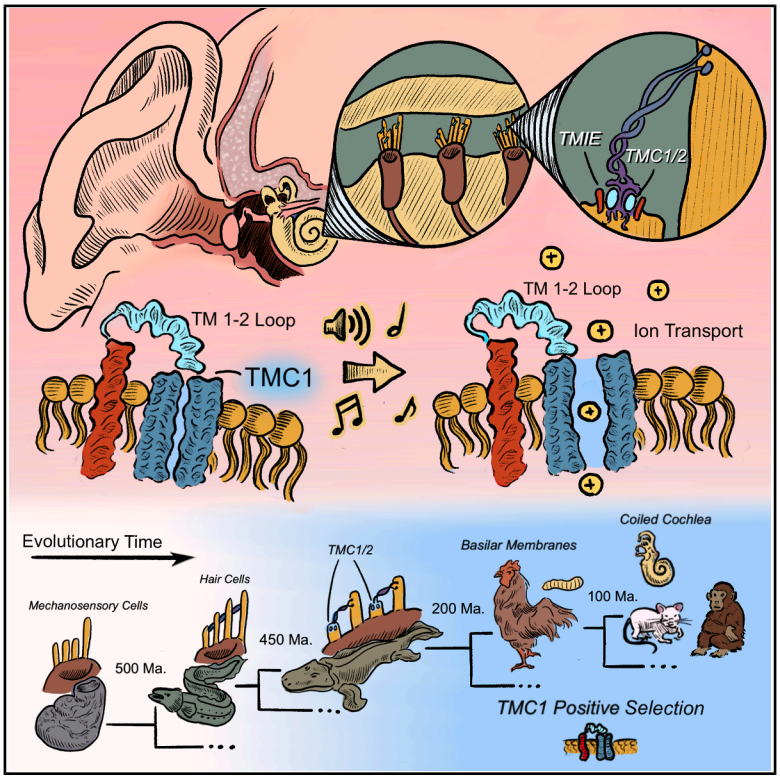

Highlights

- Lineage-specific duplications diversified the TMC family
- Positive selection targets an extracellular region (TM1-2 loop) in mammalian TMC1
- Structural models place the TM1-2 loop near the pore and the auxiliary protein TMIE
- Amino acid substitutions within this region shift TMC1 activation in hair cells

Authors

Nurunisa Akyuz, Trey J. Scott, Corena Loeb, ..., Charles B. Phillips, Nicholas W. Bellono, David P. Corey

Correspondence

nneyzi@gmail.com (N.A.), david_corey@hms.harvard.edu (D.P.C.)

In brief

Integrating evolutionary analysis, structural modeling, and electrophysiology, Akyuz et al. show that TMC1 and TMC2 arose by gene duplication and evolved specialized extracellular regions. In TMC1, an extracellular segment (the TM1-2 loop) is under positive selection in mammals, harbors deafness variants, and mutations within this region alter channel activation in native hair cells.

Akyuz et al., 2026, Current Biology *36*, 1–11
April 6, 2026
https://doi.org/10.1016/j.cub.2026.02.059

CellPress

Please cite this article in press as: Akyuz et al., Evolutionary tuning of an auditory transduction channel, Current Biology (2026), https://doi.org/10.1016/j.cub.2026.02.059

Current Biology

CellPress
OPEN ACCESS

Article

Evolutionary tuning of an auditory transduction channel

Nurunisa Akyuz,[1,5,6,*] Trey J. Scott,[2,3,5] Corena Loeb,[1,4,5] Bifeng Pan,[1,5] Yaqiao Li,[1] Charles B. Phillips,[1] Nicholas W. Bellono,[3] and David P. Corey[1,*]

[1]Department of Neurobiology, Harvard Medical School, Boston, MA 02115, USA
[2]Department of Organismic and Evolutionary Biology, Harvard University, Cambridge, MA 02138, USA
[3]Department of Molecular and Cellular Biology, Harvard University, Cambridge, MA 02138, USA
[4]Program in Speech and Hearing Bioscience and Technology, Harvard University, Cambridge, MA 02138, USA
[5]These authors contributed equally
[6]Lead contact
*Correspondence: nneyzi@gmail.com (N.A.), david_corey@hms.harvard.edu (D.P.C.)
https://doi.org/10.1016/j.cub.2026.02.059

SUMMARY

TMC1 and TMC2 are mechanosensory ion channels of the vertebrate inner ear that mediate hearing and balance. How these channels open in response to mechanical force remains unresolved. Through comparative analyses of TMCs across eukaryote species, we find that TMC1 and TMC2 arose in vertebrates by gene duplication and evolved elaborate extracellular loops. Structural models demonstrate that the loop between transmembrane domains 1 and 2 arches over the channel pore and lies near TMIE, an auxiliary protein essential for function. In mammals, this loop shows signatures of positive selection and contains multiple sites linked to hereditary deafness, consistent with TMC1's specialization for auditory function. Electrophysiological recordings from mouse *Tmc1*/*Tmc2*-null cochlear hair cells expressing TMC1 variants demonstrate that alterations within this loop affect channel activation, identifying it as a modulatory feature that has been refined through structural adaptation.

INTRODUCTION

Hearing represents a remarkable feat of evolution. Mammalian cochleae can detect sound frequencies ranging from ~15 Hz to over 100 kHz and respond to pressure waves that move the eardrum by less than the width of an atom.[1] This extraordinary sensitivity is mediated by inner ear hair cells, which convert mechanical deflections of their stereocilia into electrical signals by directly opening mechanosensitive ion channels formed by transmembrane channel-like (TMC) proteins 1 and 2 (TMC1 and TMC2)[2–7] located at the stereocilia tips[1,8,9] (Figure 1A). Loss-of-function mutations in TMC1 cause profound hearing loss, and re-expression of TMC1 and TMC2 in hair cells of deaf mice restores mechanotransduction, consistent with their roles as essential components of the transduction machinery.[3,10,11]

Despite this progress, the hair-cell transduction complex remains one of the most perplexing molecular machines. Operating at the physical limits of biological speed and precision,[12,13] it integrates pore-forming channel proteins, auxiliary subunits, and the extracellular tip links that connect adjacent stereocilia into a highly specialized mechanotransduction apparatus (Figure 1A). This architecture is difficult to reproduce *in vitro*. Although TMC-dependent currents have recently been elicited in heterologous systems,[14–17] these preparations lack the native hair bundle geometry and the tip-link-based force transmission that define vertebrate mechanotransduction.[18] Similarly, recent cryo-electron microscopy (cryo-EM) structures of TMCs[19,20] are from *C. elegans*, which lack hair cells with tip links and therefore lack the specialized features associated with vertebrate hearing (Figure 1A). Thus, understanding how native TMC channels meet the demands of hearing remains a central challenge.

Evolution offers a powerful lens for probing complex molecular machines. Selective evolutionary pressure can highlight the protein regions essential for function and specialization. This approach is particularly well suited to the TMC family, whose members (TMC1–8) share a conserved dimeric ion-channel architecture with an unusual fold resembling that of transmembrane protein 16 family (TMEM16) proteins,[5,21] yet all members support distinct physiological functions.[22] In vertebrate hair cells, TMC1 and TMC2 operate within a common, tip-link-based mechanotransduction framework[3,18,23] but contribute differently across development and sensory organs, with TMC1 distinctly required for mature auditory transduction in mammals.[2,3,10,11,24] Here, we asked whether TMC1's auditory role reflects a lineage-specific specialization to reveal structural features that support auditory mechanotransduction through vertebrate evolution.

RESULTS

Structural predictions identify subfamily-specific loop specialization

To identify the structural features that distinguish TMC1 from other TMC family members, we generated AlphaFold3 models of mouse TMC1, both alone and in complex with the auxiliary proteins TMIE (transmembrane inner ear protein) and CIB2

Please cite this article in press as: Akyuz et al., Evolutionary tuning of an auditory transduction channel, Current Biology (2026), https://doi.org/10.1016/j.cub.2026.02.059

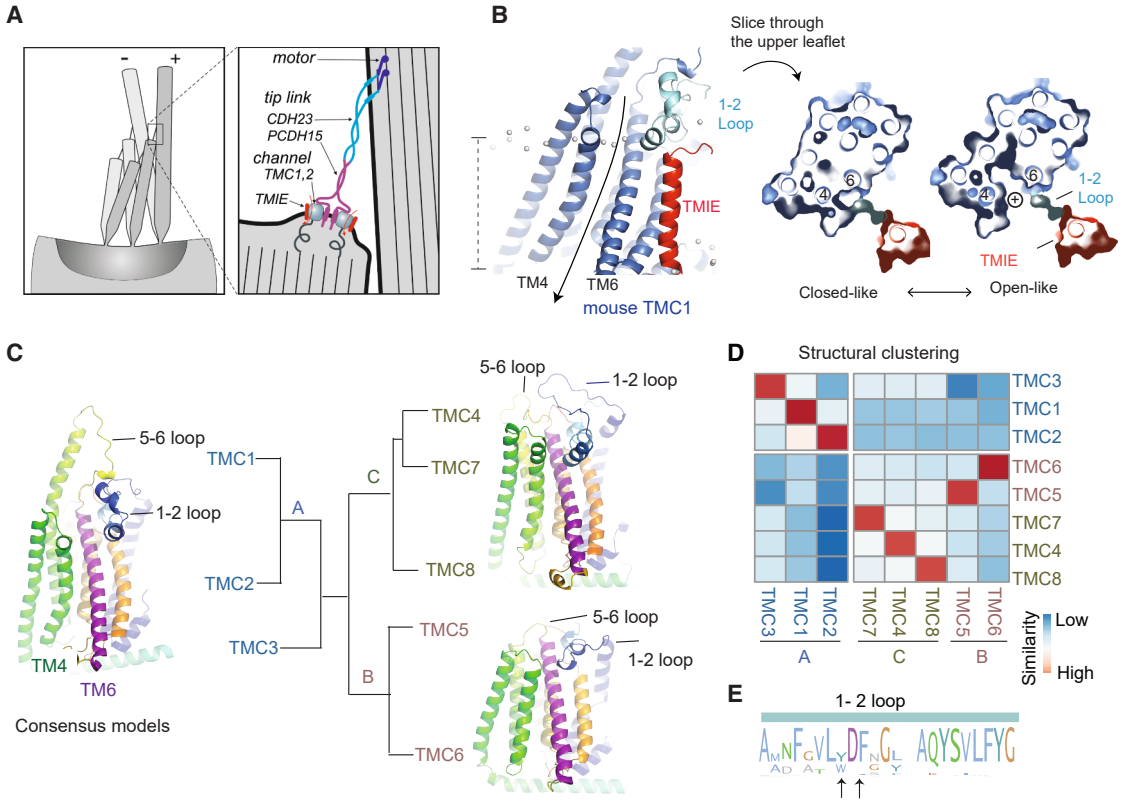

Figure 1. Evolutionary and structural insights into TMC channels

(A) Schematic of a stereociliary bundle, showing the mechanotransduction channel complex at the site of the lower tip-link insertion. Positive bundle deflection tensions the tip links, transmitting mechanical force to open the channel.

(B) Side view of an AlphaFold3 model of TMC1 in a lipid bilayer. The extracellular TM1-2 loop (cyan) arches over the pore region. The lipid headgroups (gray spheres) define the membrane boundaries. The accessory protein TMIE (red) is positioned close to the TM1-2 loop. (Right) Top-down cross-sectional surface views of the channel at the level of the outer membrane leaflet, in closed-like and open-like conformations, show the predicted widening of the pore cavity upon opening. The TM1-2 loop and nearby TMIE are indicated.

(C) AlphaFold3 models generated from extant vertebrate consensus sequences, with one representative model shown for each subfamily (see STAR Methods). The transmembrane helices are colored using a consistent PyMOL-based rainbow scheme to facilitate helix identification, with TM3 and TM4 shown in green and TM6 in purple. The TM1-2 loop (blue) consistently approaches the pore but varies in length and secondary structure. The adjacent TM5-6 loop (olive) is an extended helix in subfamily A (~40–55 residues in TMC1/2 and ~55–70 residues in TMC3), but is shorter (~5 residues) in subfamily B and intermediate (~20 residues) in subfamily C.

(D) Structural clustering of mouse TMC models separating subfamily A (cluster 1) from subfamilies B/C (cluster 2), with red representing the highest and blue the lowest similarity.

(E) Sequence logo generated from vertebrate TMC sequences, showing a highly conserved segment within the TM1-2 loop. Arrows mark the residues that were mutated for functional analysis.

See also Figures S1–S3.

(calcium- and integrin-binding protein 2). These predictions resolved the conserved ten-transmembrane core together with much of the extracellular and cytoplasmic loops with high confidence (Figures 1 and S1), providing a structural framework for comparative analysis. Among the extracellular regions, the loop linking transmembrane domains 1 and 2 (TM1-2 loop) stands out because of its strategic position above the pore-lining helices TM4 and TM6 and adjacent to TMIE (Figure 1B).[25] Evolutionary coupling analysis supports this arrangement, revealing couplings between the TM1-2 loop, pore-lining helices, and neighboring extracellular regions (Figure S2A).[25]

A comparison of predicted structures across all eight mouse *Tmc* paralogs (TMC1–8) revealed a clear pattern: while the TM1-2 loop arches over the pore in all family members, it adopts a distinctive conformation in subfamily A proteins (TMC1–3) (Figures 1C and S3A). In the same subfamily, the adjacent TM5-6 loop is also expanded and predicted to form an elongated, partly helical extracellular projection (Figures 1C and S3A). Although the distal region of this extension is predicted with lower confidence, the combined elaboration of TM1-2 and TM5-6 loops defines a distinctive extracellular architecture characteristic of TMC1–3 channels (Figure 1C).

This organization is conserved across vertebrate species. Structural models generated from consensus sequences representing extant orthologs of each vertebrate TMC subtype (see STAR Methods; Figure S3B) recapitulated the same subfamily-specific pattern, and clustering based on predicted structural similarity separated subfamily A from subfamilies B and C[26]

Please cite this article in press as: Akyuz et al., Evolutionary tuning of an auditory transduction channel, Current Biology (2026), https://doi.org/10.1016/j.cub.2026.02.059

(Figures 1D and S3C). Although this concordance between structure and phylogeny was not unexpected, it highlights that evolutionary history is inscribed in protein structure. Within subfamily A, sequence alignments of TMC1 and TMC2 revealed restricted variabilities at certain positions within the TM1-2 loop, including the conserved aromatic residues such as Y238 (Figures 1E and S2B), providing a rationale for targeted functional perturbation (below).

Evolutionary timeline reveals emergence of TMC1 and its specialized loop structures

To trace the evolutionary origins of TMC1 specialization, we mapped the presence of *Tmc* genes across a broad taxonomic range (Data S1). A maximum-likelihood gene tree resolved three canonical metazoan *Tmc* subfamilies (A, B, and C), originally defined in vertebrates[27] (Figures 2 and S4), whereas *Tmc* homologs from plants, fungi, and holozoans fall outside these subfamilies and form a distinct clade (shown in gray in Figures 2A and S4). Early-diverging metazoans, including sponges and ctenophores, retain *Tmc* genes both in this distinct clade and in lineages leading to the canonical vertebrate subfamilies (Figure S4). In contrast, cnidarians and bilaterians possess only members of the canonical subfamilies, consistent with the diversification of these subfamilies occurring prior to the cnidarians-bilaterian split and well before the emergence of vertebrate hair cells.[28] This timing coincides with a broader phase of neuronal cell type and molecular diversification in early metazoans, including sponges and ctenophores.[29,30]

Each canonical subfamily further contains nested clades of subtypes, consistent with further lineage-specific duplication events subsequently giving rise to the vertebrate paralogs (TMC1-8)[31] (Figure S4). To clarify the history of these duplications, we reconciled gene and species trees for each subfamily. In subfamily A, reconciliation is consistent with an early duplication in the chordate lineage that resulted in *Tmc3* and in a *Tmc* lineage that underwent further duplication in jawed vertebrates and resulted in both *Tmc1* and *Tmc2* (hereafter referred to as the *Tmc1/2* lineage) (Figure S5). Early-diverging subfamily A homologs, previously referred to as *Tmc123*,[31] are represented as blue squares in the *Tmc3* column in Figure 2A. The two *C. elegans* homologs, termed *tmc-1* and *tmc-2* but not closely related to vertebrate *Tmc1* and *Tmc2*, also fall within this lineage (Figure 2A).

Jawless vertebrates retain an unduplicated *Tmc* gene belonging to the *Tmc1/2* lineage (blue squares in Tmc2 column in Figure 2A) and possess typical mechanosensory hair cells in their vestibular organs.[32,33] While this does not establish a causal role, it is consistent with the possibility that *Tmc12* forms have been sufficient for early vertebrate vestibular mechanotransduction. In jawed vertebrates, *Tmc12* underwent a second duplication, giving rise to the distinct *Tmc1* and *Tmc2* clades. Thus, the *Tmc1* and *Tmc2* evolved through a two-step duplication process (*Tmc123* → *Tmc12* → *Tmc1* + *Tmc2*), with the emergence of the *Tmc12* clade coinciding with the appearance of vertebrate hair-cell mechanotransduction. Similar patterns of lineage-specific duplication and differential retention are observed in subfamilies B and C (Figure 2A; Data S2), indicating that recurrent duplication, divergence, and differential retention are common features across TMC subfamilies.

Given this duplication history, we next asked at what point in TMC evolution the distinctive extracellular features of vertebrate subfamily A were established. Comparative AlphaFold3 structural predictions reveal that early branching holozoan and metazoan lineage homologs exhibit relatively compact extracellular surfaces with minimal projections (Figure 2B). In contrast, vertebrate subfamily A members (TMC1-3) display prominent extracellular elaborations, including the curved TM1-2 loop and an extended TM5-6 projection (Figure 2B). These features are therefore not broadly conserved across early *Tmc* lineages but instead appear to have arisen along the lineage leading to the vertebrate TMC1-3, coincident with their evolutionary diversification.

Positively selected residues and clinical variants in the TM1-2 loop support functional relevance

To explore whether TMC1 functionally diverged following gene duplication, we examined patterns of selection across the *Tmc1* gene tree using a branch-site model of evolution. This analysis revealed two episodes of diversifying selection that coincided with the emergence of mammalian hearing. The first occurred along the branch leading to mammals and the second leading specifically to therian mammals (marsupials and placentals) (Figure 3A). No comparable signals were detected in *Tmc2* (Figure S6A), indicating that selective pressures acted preferentially on *Tmc1* during mammalian evolution.

To localize regions of the protein affected by these selection events, we applied a contrast fixed effects likelihood (contrast-FEL) analysis, comparing mammalian branches (foreground—blue in Figure 3A) to the remainder of the *Tmc1* gene tree (background). This revealed a general pattern of strong negative selection at the termini and positive selection within the protein core, including the TM1-2 loop (Figures 3B and 3C). The TM2-3 loop, which also showed a high proportion of positively selected residues (Figure 3B), corresponds to a well-characterized CIB2-binding domain essential for channel regulation.[34–36] By contrast, positive selection within the TM1-2 loop highlights a previously unrecognized region of potential functional importance that is specific to mammalian branches. Earlier selection events that may correspond to the transition from water to land hearing in non-mammalian tetrapods (gray square compared with rest of tree in Figure 3A) show little evidence of positive selection within this region (Figure 3B).

Consistent with its evolutionary significance, the TM1-2 loop also contains many variants identified in human TMC1 (Figures 3B and 3C). Among the 76 pathogenic or likely pathogenic single-nucleotide variants (SNVs) reported in ClinVar[37] for TMC1 (36 nonsense and 40 missense), 11 fall within this loop region, including seven missense mutations (Figure S6B). Mapping the positively selected residues in the TM1-2 loop onto a structural model of TMC1 showed that several of these cluster near the pore-lining helix TM6[5] (Figure 3C).

Targeted residue substitutions in the TM1-2 loop alter gating properties

Given its position arching over the pore, we hypothesized that the TM1-2 loop may contribute to channel gating. Guided by the structural models, we designed targeted mutations that were predicted to perturb the interactions between the TM1-2

Please cite this article in press as: Akyuz et al., Evolutionary tuning of an auditory transduction channel, Current Biology (2026), https://doi.org/10.1016/j.cub.2026.02.059

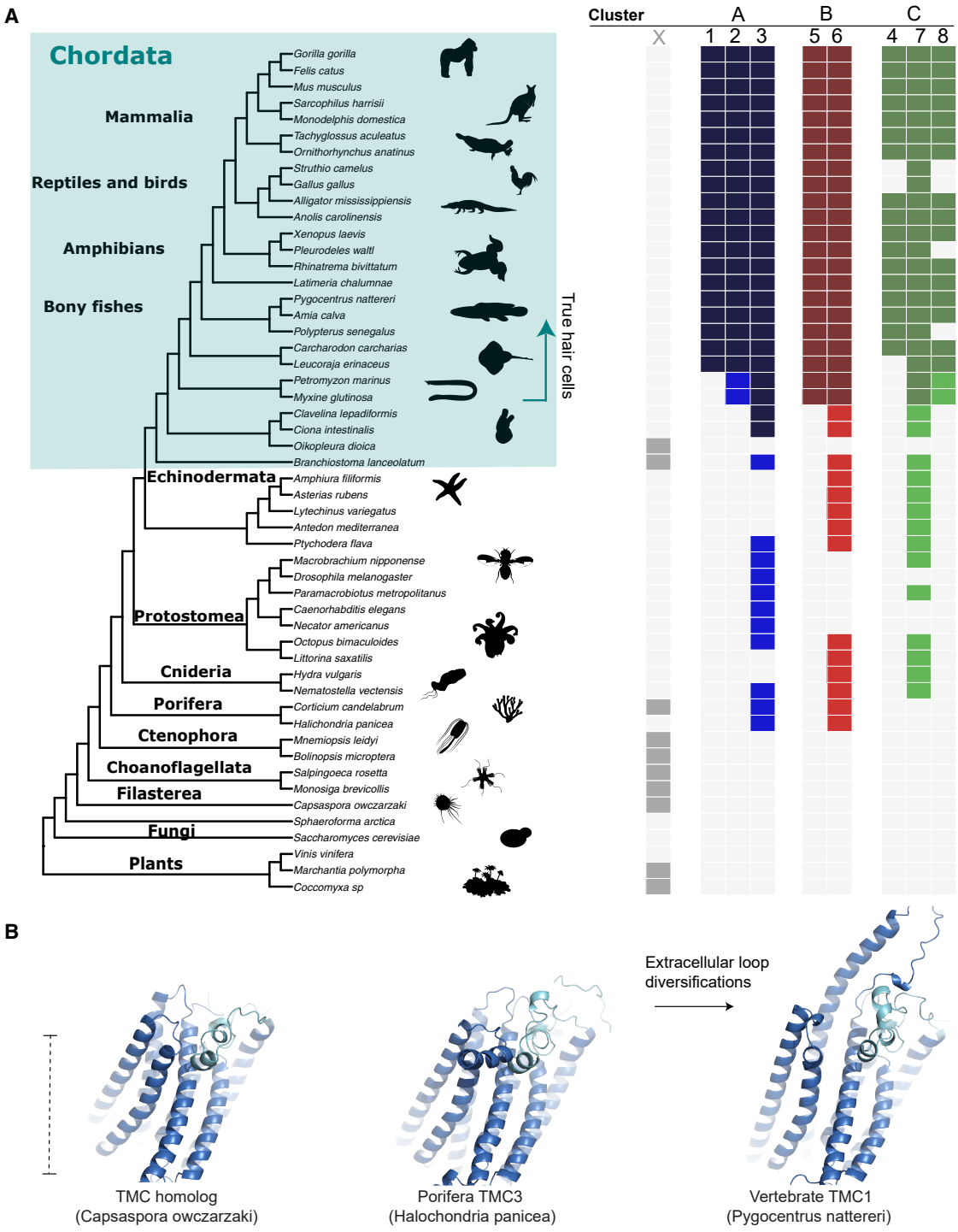

Figure 2. Expanded TMC repertoires in vertebrates

(A) Representative species tree spanning plants, fungi, unicellular holozoans, and metazoans. This tree shows topology only; branch lengths are not to scale. The grid on the right indicates the presence and subfamily assignment of *Tmc* genes present in each species (see Figures S4 and S5). Homologs are grouped into an early-diverging set (X; gray) and three metazoan subfamilies (A, B, and C). Within subfamilies A–C, canonical members are shown in darker colors and non-canonical paralogs in lighter shades (see Figure S5 and Data S2).

(B) AlphaFold3 structural models of representative extant TMC proteins from (left) early branching holozoans TMCs outside the subfamilies A, B, and C (e.g., *Capsaspora owczarzaki*), (middle) invertebrate members of the subfamily A (e.g., *Halichondria panicea*), and (right) vertebrate subfamily A channels (e.g., *Pygocentrus nattereri* TMC1), illustrating differences in extracellular domain organization.

See also Figures S4 and S5 and Data S1 and S2.

Please cite this article in press as: Akyuz et al., Evolutionary tuning of an auditory transduction channel, Current Biology (2026), https://doi.org/10.1016/j.cub.2026.02.059

CellPress
OPEN ACCESS

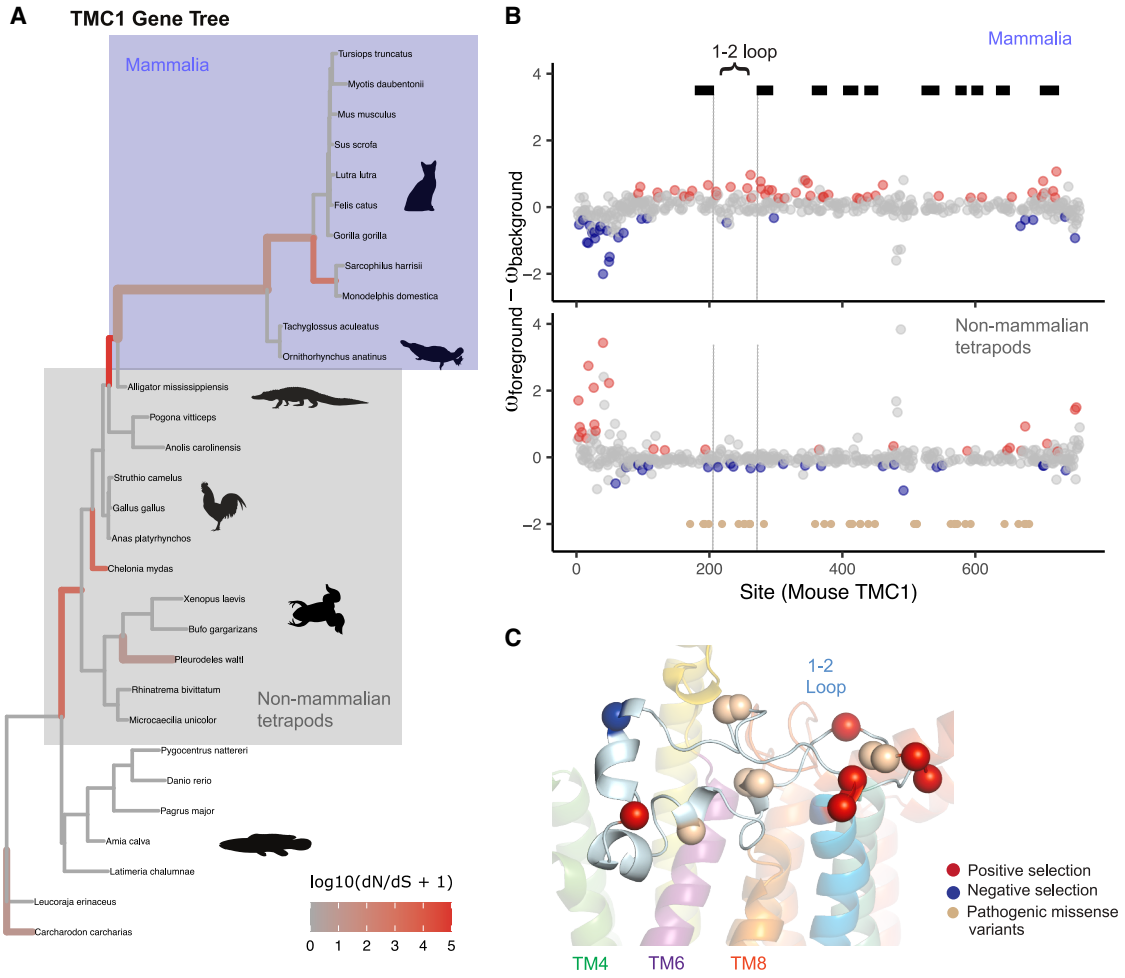

Figure 3. Mammal-specific selection within the TM1-2 loop of TMC1

(A) Gene tree of vertebrate TMC1 sequences highlighting branches under episodic diversifying selection (red). Thicker branches show more evidence for positive selection.

(B) Site-wise differences in selection pressure (ω) between background and foreground branches. The top plot shows mammalian, including therian, branches (purple shaded in A). The bottom plot shows branches associated with the water-to-land transition (gray shaded in A). Each point represents a site in mouse TMC1, plotted as Δω. Red circles indicate sites under increased positive selection, blue circles indicate sites under increased negative selection, and gray circles are sites without significant changes in foreground branches relative to background branches. Cream-colored circles at the bottom along the axis mark residues corresponding to human pathogenic variants. Black bars (top) denote predicted transmembrane regions. The location of the TM1-2 loop is indicated.

(C) Mapping, onto the structural model of TMC1, of positively selected residues (red), negatively selected residues (blue), and pathogenic missense variants (cream) within the TM1-2 loop.

See also Figure S6 and Data S3.

loop and pore-lining helices (Figure 4A). Specifically, we targeted Y238, which shows a restricted variability across vertebrates as a tyrosine in mammals and tryptophan in other vertebrates (Figure S2B), and W397 in the pore-lining helix TM4 that lies near Y238, suggesting that their interactions could influence channel gating. Using adeno-associated virus (AAV) vectors, we expressed TMC1 with mutations at Y238 and/or W397 in inner ear hair cells of Tmc1/2-null mice and used patch-clamp electrophysiology to record mechanotransduction currents in response to controlled bundle deflections (Figure 4B; STAR Methods). As reported previously,[5,25,38] AAV-expressed wild-type (WT)-TMC1 produced characteristic sigmoidal activation curves with midpoints (X_0) that were tightly aligned across recordings and similar to activation curves of WT mice, providing a robust reference for evaluating mutational effects (Table S1).

To first probe the functional role of Y238, we introduced two variants for hair-cell recordings: Y238L, which disrupts the aromatic ring while maintaining hydrophobicity, and Y238W, which preserves aromatic character but introduces a larger side chain (Figure 4A). Both mutations produced robust currents (Figure 4C) but required a greater bundle displacement for activation, consistent with a relative stabilization of closed states by the mutation (Figure 4D). Introduction of the reciprocal mutation (W290Y) into mouse TMC2 at the homologous position did not significantly shift the

Please cite this article in press as: Akyuz et al., Evolutionary tuning of an auditory transduction channel, Current Biology (2026), https://doi.org/10.1016/j.cub.2026.02.059

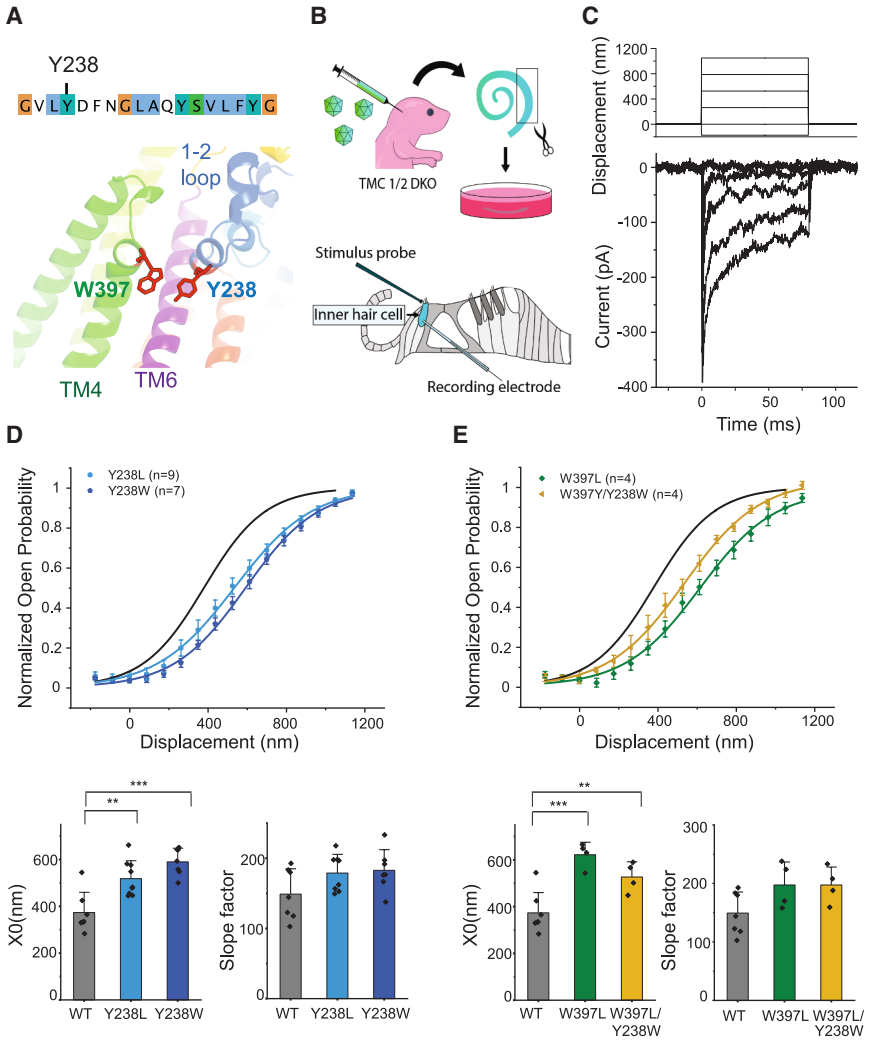

Figure 4. Mutations in the TM1-2 loop that alter gating properties

(A) Positions on the structural model of the targeted mutation sites Y238 in the extracellular TM1-2 loop and W397 in the pore-lining transmembrane helix TM4.

(B) Experimental workflow. (Top left) AAV9-PHP.B vectors encoding TMC1 variants were injected into neonatal *Tmc1/2* double-knockout (DKO) mice. (Top right) Organs of Corti were dissected and cultured. (Bottom) For hair-cell patch-clamp recordings, inner hair-cell bundles were deflected using a piezo-driven stiff glass probe.

(C) Representative transduction current traces recorded from an inner hair cell expressing the Y238L variant. The step deflections are shown at the top.

(D) (Top) Activation curves from hair cells expressing TMC1-Y238L (blue, $n = 9$) or Y238W (dark blue, $n = 7$) in comparison with the WT-TMC1 reference (black curve). The half-activation displacement (X_0) was significantly right-shifted in cells expressing Y238L (X_0 = 519 ± 25 nm) or Y238W (X_0 = 590 ± 25 nm) compared with the WT (X_0 = 380 ± 32 nm), indicating the stabilization of the closed state. Slope factors (dx) were not significantly different across groups, suggesting that the mechanical sensitivity was not altered. (Bottom) Data from multiple cells are presented as mean ± SEM. Statistical comparisons were performed using a two-tailed *t* test. Significance is indicated as follows: $p < 0.05$ (*), $p < 0.01$ (**), and $p < 0.001$ (***).

(E) The W397L mutation (green) in TM4 shifted the activation curve to the right (X_0 = 621 ± 27 nm). An aromatic swap double mutation (W397Y/Y238W, yellow) did not shift the curves further rightward (X_0 = 526 ± 30 nm). Slope factors were not significantly altered.

See also Figure S7 and Table S1.

activation curve (Figure S7A), suggesting a specificity for TMC1. Next, we targeted W397, which we predicted to interact with Y238 in the TM1-2 loop. Indeed, mutating W397 to leucine (W397L) also shifted the activation curve to the right (Figure 4E; Table S1). Collectively, these results suggest the evolutionarily specialized TM1-2 loop is important for mechanotransduction.

To test whether these residues are functionally coupled, we generated reciprocal substitutions, swapping the tryptophan and the tyrosine (Y238W/W397Y). Y238W/W397Y produced a modest leftward shift compared with W397L alone (Figure 4E), consistent with a functional coupling between these two positions. We next introduced cysteine at both positions (Y238C/W397C) to enable potential disulfide formation and impose local constraints at the TM1-2 loop/TM4 interface. This double mutant exhibited no detectable mechanotransduction currents and no FM1-43 dye entry (Figures S7B and S7C), consistent with a strong loss-of-function phenotype. While we cannot exclude that cysteine mutants could induce alternative conformational changes that impair force transmission to the pore, these results collectively demonstrate that perturbations at the TM1-2 loop/TM4 interface impact TMC1 function, consistent with a modulatory role for this extracellular region.

To explore how TM1-2 loop interactions contribute to channel gating, we examined its interfaces with auxiliary proteins, focusing on the small TMIE accessory protein, which has been implicated as a modulator of channel gating.[39] TMIE's positioning and interactions have been inferred both from the cryo-EM structures of the *C. elegans* TMC-1 and TMC-2 complexes[19,20] (Figure 5A) and from the AlphaFold3 predictions of the mammalian TMC1 channel complex (Figures 5A and S1). In these models, TMIE consistently resides at the periphery of the complex and makes direct contact with TM1-2 through F234, which is a highly conserved residue across vertebrate TMC1 orthologs. Indeed, mutating this aromatic residue to alanine (F234A) reduced force sensitivity, consistent with stabilization of the closed state (Figure 5B; Table S1). In contrast, mutation of the adjacent glycine 235 (G235A) had no effect (Figure 5B), indicating that backbone flexibility alone does not account for the gating phenotype. Together, these observations are consistent with a model in which the TM1-2 loop engages with TMIE to modulate TM4-TM6 positioning and gating.

Please cite this article in press as: Akyuz et al., Evolutionary tuning of an auditory transduction channel, Current Biology (2026), https://doi.org/10.1016/j.cub.2026.02.059

CellPress
OPEN ACCESS

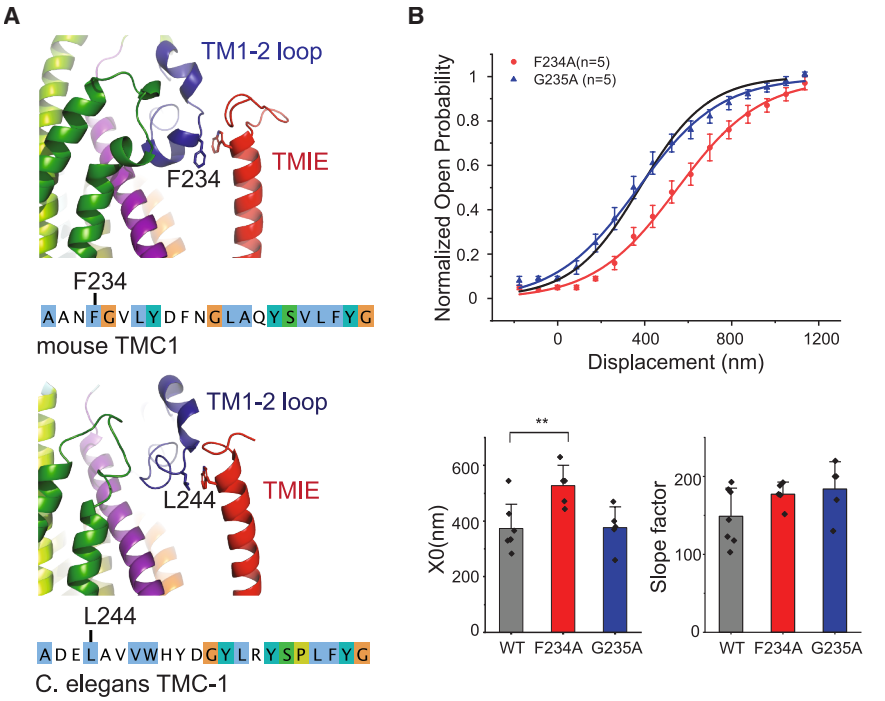

Figure 5. Mutations of residues at the TM1-2 loop/TMIE interface that affect channel gating

(A) Structural models of the TMC-TMIE complex comparing mouse TMC1 (top) and *C. elegans* TMC-1 (bottom). TMIE (red) is located at the periphery of the complex adjacent to TM6 (purple) and the TM1-2 loop (blue). In both models the TM1-2 loop is near TMIE. Residue F234 in mouse TMC1 aligns with L244 in *C. elegans*, which interacts with TMIE in the *C. elegans* cryo-EM structure (PDB: 7USX).

(B) Functional analysis of residues at the predicted TMIE and TM1-2 loop interface. The substitution of F234 with alanine (F234A, red) produced a significant rightward shift in the activation curve (X_0 = 526 ± 32 nm) relative to WT-TMC1 (black), indicating a stabilization of the closed state. The mutation of the adjacent G235 to alanine (G235A, blue) had no significant effect (X_0 = 376 ± 33 nm). Slope factors were unchanged. Data from multiple cells are presented as mean ± SEM. Significance is indicated as in Figure 4.

See also Table S1.

DISCUSSION

Evolutionary context of TMC1 and TMC2 in vertebrate hair cells

The evolution of vertebrate hearing represents a remarkable example of biological innovation, in which multiple components of the inner ear have been tuned to achieve precise mechanoelectrical conversion. Within this context, the changes in TMC proteins provide a molecular window into how natural selection may have refined auditory transduction through duplication and lineage-specific specialization. Indeed, multiple core components of the hair-cell mechanotransduction complex, including tip links (PCDH15/CDH23, protocadherin 15/cadherin 23), accessory proteins TMIE and CIB2, and the TMC1/2 channels, are shared across vertebrates, consistent with their assembly into a functional complex.[40] Notably, vestibular hair cells with tip links are found in jawless vertebrates such as hagfish, whereas earlier-diverging chordates such as lancelets (amphioxus) lack bona fide hair cells.[41] These observations are consistent with the emergence of tip-link-based mechanotransduction near the origin of vertebrates[42] and indicate that the basic molecular architecture required for hair-cell mechanosensation was established early in vertebrate evolution (Figure 6). Considering this evolutionary context, our phylogenetic analyses indicate that *Tmc1* and *Tmc2* evolved through two successive duplication events during subfamily A evolution (Figure 2): an early duplication in a chordate ancestor that is retained in jawless vertebrates, followed by a later duplication in jawed vertebrates that produced the distinct *Tmc1* and *Tmc2* paralogs. Thus, by the time of the appearance of early fishes, both proteins were already present.

Subsequent neofunctionalization of Tmc1 may have involved the move from water to land. This transition would have imposed new mechanical and sensory demands on this existing complex, with later refinements continuing through the emergence of mammals. The mammalian- and therian-specific signatures of positive selection that we identified point to further neofunctionalization in mammals that has affected the TM1-2 loop. These lineage-specific changes coincide with evolutionary intervals of auditory specialization, including the emergence of the organ of Corti, the differentiation of inner and outer hair cells,[44] and subsequent specializations such as cochlear coiling and high-frequency sensitivity[45] (Figure 6). Although our data do not establish causal links between specific morphological innovations and sequence changes, they place *Tmc1* evolution within the timeline in which molecular, structural, and physiological specializations of the mammalian cochlea arose. More broadly, these results suggest that the auditory transduction channel evolved not through the invention of new molecular components but through the repurposing and tuning of an ancestral mechanosensory architecture, which was made available by stochastic gene duplications, a recurring theme in sensory evolution.[29,46,47]

Functional consequences of TM1-2 loop perturbation

Placing the evolutionary signals in a structural context localizes branch-level patterns of selection to specific regions of TMC1 (Figures 1 and 2), in particular the TM1-2 loop. This loop is part of distinctive extracellular elaborations that are unique to subfamily A TMCs. Mutating conserved aromatic residues within the TM1-2 loop (F234 and Y238) shifted channel activation toward the closed state, indicating altered gating energetics. Because hair-cell adaptation can partially compensate for static bundle offsets, energetic shifts inferred from midpoint changes should be interpreted as the lower bounds on intrinsic gating effects (see STAR Methods). Together, these findings support a modulatory role for the TM1-2 loop in TMC1 gating energetics

Please cite this article in press as: Akyuz et al., Evolutionary tuning of an auditory transduction channel, Current Biology (2026), https://doi.org/10.1016/j.cub.2026.02.059

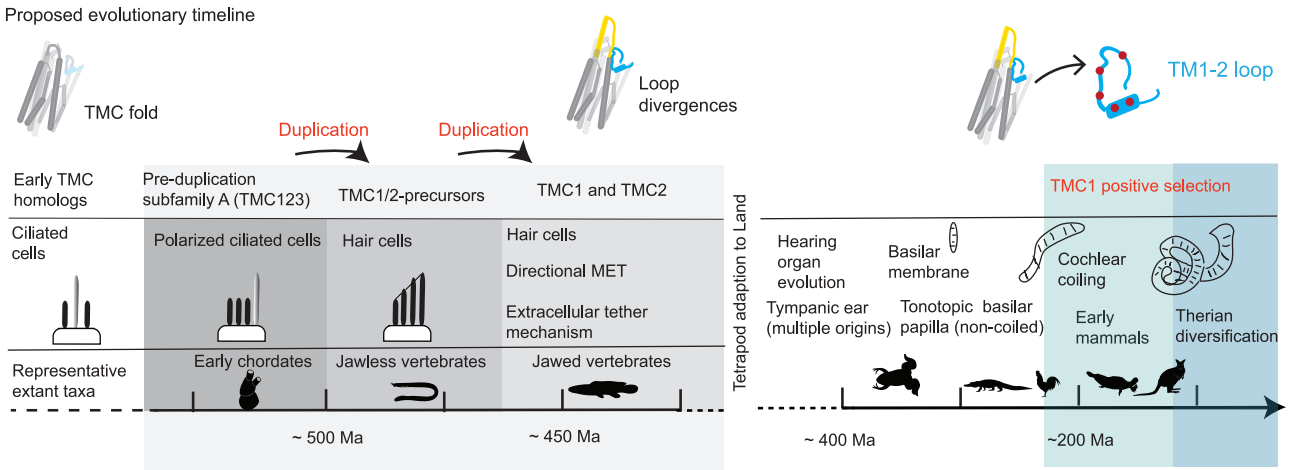

Figure 6. Evolutionary emergence and specialization of TMC1

(Top row) Structural schematics showing major transitions in the TMC1 family. (Left) The core TMC fold, retained in early-diverging TMC homologs, is conserved across the entire family. (Middle) Together with the duplication events that gave rise to canonical vertebrate TMC1–3 subtypes, elaborated extracellular loops emerged, a feature unique to vertebrate subfamily A (colored domains). (Right) In mammals, positive selection further refined TMC1, with one hotspot of changes in the TMC1-2 loop (blue, selected sites in red).

(Second row) Two successive gene duplication events within a *Tmc3*-like (*Tmc123*) lineage first produced a *Tmc1/2* precursor and subsequently the distinct *Tmc1* and *Tmc2* paralogs.

(Third row) A previously established evolutionary timeline showing the transitions from non-polarized sensory cells to mechanosensory cells, vestibular hair cells, and eventually cochlear hair cells specialized for hearing.[43] Key auditory innovations include a tympanic ear, tonotopic basilar papilla, and cochlear coiling. The animal silhouettes along the bottom represent the approximate timing of major divergences of species, including early chordates, jawless vertebrates, jawed vertebrates, tetrapods, early mammals, and therian mammals. The light blue shaded region highlights the period of positive selection in TMC1 coinciding with cochlear coiling and other specializations associated with mammalian hearing.

in a paralog-specific manner. Although consistent with tethered-gating models in which extracellular linkages bias the channel's open-closed equilibrium through mechanical tension,[18,48] additional data will be needed to establish whether this region contributed to tip-link-mediated force transmission.

Substitutions within the TM1-2 loop likely disrupt the delicate network linking the loop, TM4, TM6, and TMIE, which may help to explain why pathogenic mutations associated with autosomal dominant or recessive non-syndromic hearing loss cluster here (Figure S6B). In combination with previously reported evolutionary analyses showing the lineage-specific tuning of interactions with the tip-links protein PCDH15-CDH23,[40] these results suggest that both the extracellular force-transmission apparatus and the channel itself appear to have been shaped by evolution. Whether these adaptations occurred in concert, maintaining effective coupling between TMC1 and PCDH15, remains an open question.

Modular specialization of TMC proteins

The evolutionary patterns observed for the TM1-2 loop fit within a broader view of TMC proteins as modular channels. The conserved ten-transmembrane core provides a stable scaffold, while the more variable extracellular and cytoplasmic regions act as tunable interfaces that can adapt to diverse mechanical or chemical environments. In *C. elegans*, a single TMC-1 protein mediates both mechanosensation and alkaline sensing through distinct structural domains.[22] In vertebrates, these functions are partitioned between paralogs: TMC1 is responsible for mechanosensation function and TMC3 for alkaline sensing,[22] reflecting a modular, domain-specific mode of molecular evolution. The evolutionary specialization of *Tmc1* for auditory function is also consistent with broader trends of adaptive evolution among inner-ear-expressed genes.[49] Within this framework, the TM1-2 loop represents a peripheral domain that is conserved within subfamily A but has undergone lineage-specific refinement. In this context, comparative analyses of TMC proteins across species and sensory modalities[50–53] provide a means to link molecular adaptations to changes in sensory function. For example, convergent substitutions in *Tmc1* have been identified in distantly related echolocating species such as bats and oilbirds, pointing to common adaptive pressure on this channel.[54]

RESOURCE AVAILABILITY

Lead contact

Requests for further information and resources should be directed to and will be fulfilled by the lead contact, Nurunisa Akyuz (nneyzi@gmail.com).

Materials availability

All unique reagents generated are available from the lead contact and will be provided by the Corey Lab at Harvard Medical School upon completion of a materials transfer agreement.

Data and code availability

- The complete set of alignments, including those used for selection analyses and reconciliations, has been deposited in a public repository (https://gitlab.com/treyjscott/tmc) and is publicly available.
- This paper does not report original code.
- Any additional data required to reanalyze the data reported in this paper are available from the lead contact upon request.

ACKNOWLEDGMENTS

We thank members of the Corey laboratory for discussions and support, Drs. Olga Boudker and Richard Losick for critical reading of the manuscript, Yiming Zhang at Boston Children's Hospital Viral Core for producing AAV vectors, Bruce Derfler for assistance with reagents, and Drs. Andrew Griffith and Jeffrey Holt for providing $Tmc1^{\Delta/\Delta}$/$Tmc2^{\Delta/\Delta}$ mice.[2] This work was supported by the National Institutes of Health (NIDCD R01 DC000304 to D.P.C.), an American Hearing Research Foundation (AHRF) discovery grant (to N.A.), and a Harvard Brain Science Initiative Postdoctoral Pioneers grant (to N.A.). T.S. is a fellow of the Jane Coffin Childs Memorial Fund for Medical Research. C.L. is supported by the Stuart H.Q. and Victoria Quan Fellowship and by the National Institutes of Health (NIDCD T32 DC000038 to G. Géléoc).

AUTHOR CONTRIBUTIONS

Conceptualization, N.A. and T.S.; methodology, N.A., T.S., B.P., C.L., Y.L., and C.B.P.; investigation, N.A. (construct generation and preparation), B.P. (hair-cell electrophysiology recordings), C.L. (cochlear dissections and FM1-43 uptake), Y.L. (animal breeding and cochlear injections), and T.S. (evolutionary data curation); formal analysis, N.A. (electrophysiology data analysis and structural modeling) and T.S. (evolutionary analyses); visualization, N.A. and T.S.; writing—original draft, N.A. and T.S.; writing—review & editing, N.A., T.S., N.W.B., and D.P.C.; resources, D.P.C.; supervision, D.P.C.

DECLARATION OF INTERESTS

The authors declare no competing interests.

STAR★METHODS

Detailed methods are provided in the online version of this paper and include the following:

- KEY RESOURCES TABLE
- EXPERIMENTAL MODEL AND STUDY PARTICIPANT DETAILS
  - Mouse strains
- METHOD DETAILS
  - Consensus sequence generation
  - Structure prediction and similarity analysis
  - Evolution of TMC subfamilies
  - Evolutionary selection analysis
  - AAV vector preparations
  - AAV virus injections
  - Cochlear dissection
  - FM1-43 dye uptake assay
  - Electrophysiology
- QUANTIFICATION AND STATISTICAL ANALYSIS

SUPPLEMENTAL INFORMATION

Supplemental information can be found online at https://doi.org/10.1016/j.cub.2026.02.059.

Received: October 23, 2025
Revised: December 1, 2025
Accepted: February 26, 2026

REFERENCES

1. Hudspeth, A.J. (1989). How the ear's works work. Nature *341*, 397–404. https://doi.org/10.1038/341397a0.
2. Kawashima, Y., Géléoc, G.S.G., Kurima, K., Labay, V., Lelli, A., Asai, Y., Makishima, T., Wu, D.K., Della Santina, C.C., Holt, J.R., et al. (2011). Mechanotransduction in mouse inner ear hair cells requires transmembrane channel-like genes. J. Clin. Investig. *121*, 4796–4809. https://doi.org/10.1172/JCI60405.
3. Pan, B., Géléoc, G.S., Asai, Y., Horwitz, G.C., Kurima, K., Ishikawa, K., Kawashima, Y., Griffith, A.J., and Holt, J.R. (2013). Tmc1 and tmc2 are components of the mechanotransduction channel in hair cells of the mammalian inner ear. Neuron *79*, 504–515. https://doi.org/10.1016/j.neuron.2013.06.019.
4. Corns, L.F., Johnson, S.L., Kros, C.J., and Marcotti, W. (2016). Tmc1 point mutation affects ca2+ sensitivity and block by dihydrostreptomycin of the mechanoelectrical transducer current of mouse outer hair cells. J. Neurosci. *36*, 336–349. https://doi.org/10.1523/JNEUROSCI.2439-15.2016.
5. Pan, B., Akyuz, N., Liu, X.P., Asai, Y., Nist-Lund, C., Kurima, K., Derfler, B.H., György, B., Limapichat, W., Walujkar, S., et al. (2018). Tmc1 forms the pore of mechanosensory transduction channels in vertebrate inner ear hair cells. Neuron *99*, 736–753.e6. https://doi.org/10.1016/j.neuron.2018.07.033.
6. Kurima, K., Peters, L.M., Yang, Y., Riazuddin, S., Ahmed, Z.M., Naz, S., Arnaud, D., Drury, S., Mo, J., Makishima, T., et al. (2002). Dominant and recessive deafness caused by mutations of a novel gene, tmc1, required for cochlear hair-cell function. Nat. Genet. *30*, 277–284. https://doi.org/10.1038/ng842.
7. Vreugde, S., Erven, A., Kros, C.J., Marcotti, W., Fuchs, H., Kurima, K., Wilcox, E.R., Friedman, T.B., Griffith, A.J., Balling, R., et al. (2002). Beethoven, a mouse model for dominant, progressive hearing loss dfna36. Nat. Genet. *30*, 257–258. https://doi.org/10.1038/ng848.
8. Gillespie, P.G., and Müller, U. (2009). Mechanotransduction by hair cells: Models, molecules, and mechanisms. Cell *139*, 33–44. https://doi.org/10.1016/j.cell.2009.09.010.
9. Fettiplace, R. (2020). Diverse mechanisms of sound frequency discrimination in the vertebrate cochlea. Trends Neurosci. *43*, 88–102. https://doi.org/10.1016/j.tins.2019.12.003.
10. Asai, Y., Pan, B., Nist-Lund, C., Galvin, A., Lukashkin, A.N., Lukashkina, V.A., Chen, T., Zhou, W., Zhu, H., Russell, I.J., et al. (2018). Transgenic tmc2 expression preserves inner ear hair cells and vestibular function in mice lacking tmc1. Sci. Rep. *8*, 12124. https://doi.org/10.1038/s41598-018-28958-x.
11. Nakanishi, H., Kurima, K., Pan, B., Wangemann, P., Fitzgerald, T.S., Géléoc, G.S., Holt, J.R., and Griffith, A.J. (2018). Tmc2 expression partially restores auditory function in a mouse model of dfnb7/b11 deafness caused by loss of tmc1 function. Sci. Rep. *8*, 12125. https://doi.org/10.1038/s41598-018-29709-8.
12. Fettiplace, R., Crawford, A.C., and Evans, M.G. (1992). The hair cell's mechanoelectrical transducer channel. Ann. N. Y. Acad. Sci. *656*, 1–11. https://doi.org/10.1111/j.1749-6632.1992.tb25196.x.
13. Bialek, W., and Schweitzer, A. (1985). Quantum noise and the threshold of hearing. Phys. Rev. Lett. *54*, 725. https://doi.org/10.1103/PhysRevLett.54.725.
14. Fu, S., Pan, X., Lu, M., Dong, J., and Yan, Z. (2025). Human tmc1 and tmc2 are mechanically gated ion channels. Neuron *113*, 411–425.e4. https://doi.org/10.1016/j.neuron.2024.11.009.
15. Chen, Y., Li, Y., Liu, Y., Sun, J., Feng, W., Chen, Y., Tian, Y., Lei, T., and Huang, P. (2025). Ectopic mouse tmc1 and tmc2 alone form mechanosensitive channels that are potently modulated by tmie. Proc. Natl. Acad. Sci. USA *122*, e2403141122. https://doi.org/10.1073/pnas.2403141122.
16. Jia, Y., Zhao, Y., Kusakizako, T., Wang, Y., Pan, C., Zhang, Y., Nureki, O., Hattori, M., and Yan, Z. (2020). Tmc1 and tmc2 proteins are pore-forming subunits of mechanosensitive ion channels. Neuron *105*, 310–321.e3. https://doi.org/10.1016/j.neuron.2019.10.017.
17. Deng, S., and Yan, Z. (2025). Tmc1 and tmc2 function as the mechanoelectrical transduction ion channel in hearing. Curr. Opin. Neurobiol. *93*, 103026. https://doi.org/10.1016/j.conb.2025.103026.
18. Pickles, J.O., Comis, S.D., and Osborne, M.P. (1984). Cross-links between stereocilia in the guinea pig organ of corti, and their possible relation to

sensory transduction. Hear. Res. *15*, 103–112. https://doi.org/10.1016/0378-5955(84)90041-8.

19. Jeong, H., Clark, S., Goehring, A., Dehghani-Ghahnaviyeh, S., Rasouli, A., Tajkhorshid, E., and Gouaux, E. (2022). Structures of the tmc-1 complex illuminate mechanosensory transduction. Nature *610*, 796–803. https://doi.org/10.1038/s41586-022-05314-8.
20. Clark, S., Jeong, H., Posert, R., Goehring, A., and Gouaux, E. (2024). The structure of the caenorhabditis elegans tmc-2 complex suggests roles of lipid-mediated subunit contacts in mechanosensory transduction. Proc. Natl. Acad. Sci. USA *121*, e2314096121. https://doi.org/10.1073/pnas.2314096121.
21. Ballesteros, A., Fenollar-Ferrer, C., and Swartz, K.J. (2018). Structural relationship between the putative hair cell mechanotransduction channel tmc1 and tmem16 proteins. eLife *7*, e38433. https://doi.org/10.7554/eLife.38433.
22. Jiang, Q., Zou, W., Li, S., Qiu, X., Zhu, L., Kang, L., and Müller, U. (2024). Sequence variations and accessory proteins adapt tmc functions to distinct sensory modalities. Neuron *112*, 2922–2937.e8. https://doi.org/10.1016/j.neuron.2024.06.013.
23. Holt, J.R., Tobin, M., Elferich, J., Gouaux, E., Ballesteros, A., Yan, Z., Ahmed, Z.M., and Nicolson, T. (2021). Putting the pieces together: The hair cell transduction complex. J. Assoc. Res. Otolaryngol. *22*, 601–608. https://doi.org/10.1007/s10162-021-00808-0.
24. Marcovich, I., and Holt, J.R. (2020). Evolution and function of tmc genes in mammalian hearing. Curr. Opin. Physiol. *18*, 11–19. https://doi.org/10.1016/j.cophys.2020.06.011.
25. Akyuz, N., Karavitaki, K.D., Pan, B., Tamvakologos, P.I., Brock, K.P., Li, Y., Marks, D.S., and Corey, D.P. (2022). Mechanical gating of the auditory transduction channel tmc1 involves the fourth and sixth transmembrane helices. Sci. Adv. *8*, eabo1126. https://doi.org/10.1126/sciadv.abo1126.
26. Zhang, Y., and Skolnick, J. (2005). Tm-align: A protein structure alignment algorithm based on the tm-score. Nucleic Acids Res. *33*, 2302–2309. https://doi.org/10.1093/nar/gki524.
27. Keresztes, G., Mutai, H., and Heller, S. (2003). Tmc and ever genes belong to a larger novel family, the tmc gene family encoding transmembrane proteins. BMC Genomics *4*, 24. https://doi.org/10.1186/1471-2164-4-24.
28. Schlosser, G. (2018). A short history of nearly every sense-the evolutionary history of vertebrate sensory cell types. Integr. Comp. Biol. *58*, 301–316. https://doi.org/10.1093/icb/icy024.
29. Arendt, D. (2008). The evolution of cell types in animals: Emerging principles from molecular studies. Nat. Rev. Genet. *9*, 868–882. https://doi.org/10.1038/nrg2416.
30. Arendt, D., Bertucci, P.Y., Achim, K., and Musser, J.M. (2019). Evolution of neuronal types and families. Curr. Opin. Neurobiol. *56*, 144–152. https://doi.org/10.1016/j.conb.2019.01.022.
31. Erives, A., and Fritzsch, B. (2020). A screen for gene paralogies delineating evolutionary branching order of early metazoa. G3 (Bethesda) *10*, 811–826. https://doi.org/10.1534/g3.119.400951.
32. Fritzsch, B., Kersigo, J., Rejent, K., Gherman, W., Frank, P.W., Giovannucci, D.R., and Maklad, A. (2023). Hair cell morphological patterns and polarity organization in the sea lamprey vestibular cristae. Anat. Rec. (Hoboken) *306*, 2170–2184. https://doi.org/10.1002/ar.25164.
33. Maklad, A., Reed, C., Johnson, N.S., and Fritzsch, B. (2014). Anatomy of the lamprey ear: Morphological evidence for occurrence of horizontal semicircular ducts in the labyrinth of petromyzon marinus. J. Anat. *224*, 432–446. https://doi.org/10.1111/joa.12159.
34. Liang, X., Qiu, X., Dionne, G., Cunningham, C.L., Pucak, M.L., Peng, G., Kim, Y.H., Lauer, A., Shapiro, L., and Müller, U. (2021). Cib2 and cib3 are auxiliary subunits of the mechanotransduction channel of hair cells. Neuron *109*, 2131–2149.e15. https://doi.org/10.1016/j.neuron.2021.05.007.
35. Giese, A.P.J., Weng, W.H., Kindt, K.S., Chang, H.H.V., Montgomery, J.S., Ratzan, E.M., Beirl, A.J., Rivera, R.A., Lotthammer, J.M., Walujkar, S., et al. (2025). Complexes of vertebrate TMC1/2 and CIB2/3 proteins form hair-cell mechanotransduction cation channels. Elife *12*. https://doi.org/10.7554/eLife.89719.
36. Giese, A.P.J., Tang, Y.Q., Sinha, G.P., Bowl, M.R., Goldring, A.C., Parker, A., Freeman, M.J., Brown, S.D.M., Riazuddin, S., Fettiplace, R., et al. (2017). Cib2 interacts with tmc1 and tmc2 and is essential for mechanotransduction in auditory hair cells. Nat. Commun. *8*, 43. https://doi.org/10.1038/s41467-017-00061-1.
37. Landrum, M.J., and Kattman, B.L. (2018). Clinvar at five years: Delivering on the promise. Hum. Mutat. *39*, 1623–1630. https://doi.org/10.1002/humu.23641.
38. Lee, J., Nist-Lund, C., Solanes, P., Goldberg, H., Wu, J., Pan, B., Schneider, B.L., and Holt, J.R. (2020). Efficient viral transduction in mouse inner ear hair cells with utricle injection and aav9-php.B. Hear. Res. *394*, 107882. https://doi.org/10.1016/j.heares.2020.107882.
39. Cunningham, C.L., Qiu, X., Wu, Z., Zhao, B., Peng, G., Kim, Y.H., Lauer, A., and Müller, U. (2020). Tmie defines pore and gating properties of the mechanotransduction channel of mammalian cochlear hair cells. Neuron *107*, 126–143.e8. https://doi.org/10.1016/j.neuron.2020.03.033.
40. Nisler, C.R., Narui, Y., Scheib, E., Choudhary, D., Bowman, J.D., Mandayam Bharathi, H., Lynch, V.J., and Sotomayor, M. (2023). Interpreting the evolutionary echoes of a protein complex essential for inner-ear mechanosensation. Mol. Biol. Evol. *40*, msad057. https://doi.org/10.1093/molbev/msad057.
41. Fritzsch, B., and Glover, J.C. (2024). Gene networks and the evolution of olfactory organs, eyes, hair cells and motoneurons: A view encompassing lancelets, tunicates and vertebrates. Front. Cell Dev. Biol. *12*, 1340157. https://doi.org/10.3389/fcell.2024.1340157.
42. Fritzsch, B., Beisel, K.W., Pauley, S., and Soukup, G. (2007). Molecular evolution of the vertebrate mechanosensory cell and ear. Int. J. Dev. Biol. *51*, 663–678. https://doi.org/10.1387/ijdb.072367bf.
43. Fritzsch, B., and Straka, H. (2014). Evolution of vertebrate mechanosensory hair cells and inner ears: Toward identifying stimuli that select mutation driven altered morphologies. J. Comp. Physiol. A Neuroethol. Sens. Neural Behav. Physiol. *200*, 5–18. https://doi.org/10.1007/s00359-013-0865-z.
44. Köppl, C., and Manley, G.A. (2019). A functional perspective on the evolution of the cochlea. Cold Spring Harb. Perspect. Med. *9*, a033241. https://doi.org/10.1101/cshperspect.a033241.
45. Manley, G.A. (2017). Comparative auditory neuroscience: Understanding the evolution and function of ears. J. Assoc. Res. Otolaryngol. *18*, 1–24. https://doi.org/10.1007/s10162-016-0579-3.
46. Oakley, T.H., and Speiser, D.I. (2015). How complexity originates: The evolution of animal eyes. Annu. Rev. Ecol. Evol. Syst. *46*, 237–260. https://doi.org/10.1146/annurev-ecolsys-110512-135907.
47. Valencia-Montoya, W.A., Pierce, N.E., and Bellono, N.W. (2024). Evolution of sensory receptors. Annu. Rev. Cell Dev. Biol. *40*, 353–379. https://doi.org/10.1146/annurev-cellbio-120123-112853.
48. Assad, J.A., Shepherd, G.M., and Corey, D.P. (1991). Tip-link integrity and mechanical transduction in vertebrate hair cells. Neuron *7*, 985–994. https://doi.org/10.1016/0896-6273(91)90343-x.
49. Pisciottano, F., Cinalli, A.R., Stopiello, J.M., Castagna, V.C., Elgoyhen, A.B., Rubinstein, M., Gómez-Casati, M.E., and Franchini, L.F. (2019). Inner ear genes underwent positive selection and adaptation in the mammalian lineage. Mol. Biol. Evol. *36*, 1653–1670. https://doi.org/10.1093/molbev/msz077.
50. Kasahara, Y., Narukawa, M., Saito, Y., Abe, K., and Asakura, T. (2024). The complexities of salt taste reception: Insights into the role of tmc4 in chloride taste detection. Front. Mol. Neurosci. *17*, 1468438. https://doi.org/10.3389/fnmol.2024.1468438.
51. Ebrahim, S., Ballesteros, A., Zheng, W.S., Mukherjee, S., Hu, G., Weng, W.H., Montgomery, J.S., Agyemang, Y., Cui, R., Sun, W., et al. (2024). Transmembrane channel-like 4 and 5 proteins at microvillar tips are potential ion channels and lipid scramblases. Preprint at bioRxiv. https://doi.org/10.1101/2024.08.22.609173.

52. Kortmann, J., Huang, K., Tsai, M.-C., Barck, K., Jacobson, A., Austin, C.D., Dunlap, D., Chalouni, C., Jeet, S., Balestrini, A., et al. (2023). Lung-innervating neurons expressing tmc3 can induce broncho-constriction and dilation with direct consequences for the respiratory cycle. Preprint at bioRxi. https://doi.org/10.1101/2023.08.24.554567.

53. Koehler, K.R., Nie, J., Longworth-Mills, E., Liu, X.P., Lee, J., Holt, J.R., and Hashino, E. (2017). Generation of inner ear organoids containing functional hair cells from human pluripotent stem cells. Nat. Biotechnol. *35*, 583–589. https://doi.org/10.1038/nbt.3840.

54. Sadanandan, K.R., Ko, M.C., Low, G.W., Gahr, M., Edwards, S.V., Hiller, M., Sackton, T.B., Rheindt, F.E., Sin, S.Y.W., and Baldwin, M.W. (2023). Convergence in hearing-related genes between echolocating birds and mammals. Proc. Natl. Acad. Sci. USA *120*, e2307340120. https://doi.org/10.1073/pnas.2307340120.

55. Katoh, K., and Standley, D.M. (2013). Mafft multiple sequence alignment software version 7: Improvements in performance and usability. Mol. Biol. Evol. *30*, 772–780. https://doi.org/10.1093/molbev/mst010.

56. Nguyen, L.T., Schmidt, H.A., von Haeseler, A., and Minh, B.Q. (2015). Iq-tree: A fast and effective stochastic algorithm for estimating maximum-likelihood phylogenies. Mol. Biol. Evol. *32*, 268–274. https://doi.org/10.1093/molbev/msu300.

57. Pond, S.L.K., Frost, S.D.W., and Muse, S.V. (2005). Hyphy: Hypothesis testing using phylogenies. Bioinformatics *21*, 676–679. https://doi.org/10.1093/bioinformatics/bti079.

58. Hernández-Plaza, A., Deng, Z., Robledo-Yagüe, F., Szklarczyk, D., von Mering, C., Bork, P., and Huerta-Cepas, J. (2026). Eggnog v7: Phylogeny-based orthology predictions and functional annotations. Nucleic Acids Res. *54*, D402–D408. https://doi.org/10.1093/nar/gkaf1249.

59. Metsalu, T., and Vilo, J. (2015). Clustvis: A web tool for visualizing clustering of multivariate data using principal component analysis and heatmap. Nucleic Acids Res. *43*, W566–W570. https://doi.org/10.1093/nar/gkv468.

60. Emms, D.M., and Kelly, S. (2019). Orthofinder: Phylogenetic orthology inference for comparative genomics. Genome Biol. *20*, 238. https://doi.org/10.1186/s13059-019-1832-y.

61. Zhang, C., Nielsen, R., and Mirarab, S. (2025). Aster: A package for large-scale phylogenomic reconstructions. Mol. Biol. Evol. *42*, msaf172. https://doi.org/10.1093/molbev/msaf172.

62. Morel, B., Kozlov, A.M., Stamatakis, A., and Szöllősi, G.J. (2020). Generax: A tool for species-tree-aware maximum likelihood-based gene family tree inference under gene duplication, transfer, and loss. Mol. Biol. Evol. *37*, 2763–2774. https://doi.org/10.1093/molbev/msaa141.

63. Suyama, M., Torrents, D., and Bork, P. (2006). Pal2nal: Robust conversion of protein sequence alignments into the corresponding codon alignments. Nucleic Acids Res. *34*, W609–W612. https://doi.org/10.1093/nar/gkl315.

64. Sievers, F., and Higgins, D.G. (2021). The clustal omega multiple alignment package. Methods Mol. Biol. *2231*, 3–16. https://doi.org/10.1007/978-1-0716-1036-7_1.

65. Waterhouse, A.M., Procter, J.B., Martin, D.M.A., Clamp, M., and Barton, G.J. (2009). Jalview version 2--a multiple sequence alignment editor and analysis workbench. Bioinformatics *25*, 1189–1191. https://doi.org/10.1093/bioinformatics/btp033.

66. Abramson, J., Adler, J., Dunger, J., Evans, R., Green, T., Pritzel, A., Ronneberger, O., Willmore, L., Ballard, A.J., Bambrick, J., et al. (2024). Accurate structure prediction of biomolecular interactions with alphafold 3. Nature *630*, 493–500. https://doi.org/10.1038/s41586-024-07487-w.

67. Mistry, J., Chuguransky, S., Williams, L., Qureshi, M., Salazar, G.A., Sonnhammer, E.L.L., Tosatto, S.C.E., Paladin, L., Raj, S., Richardson, L.J., et al. (2021). Pfam: The protein families database in 2021. Nucleic Acids Res. *49*, D412–D419. https://doi.org/10.1093/nar/gkaa913.

68. Kalyaanamoorthy, S., Minh, B.Q., Wong, T.K.F., von Haeseler, A., and Jermiin, L.S. (2017). Modelfinder: Fast model selection for accurate phylogenetic estimates. Nat. Methods *14*, 587–589. https://doi.org/10.1038/nmeth.4285.

69. Hoang, D.T., Chernomor, O., von Haeseler, A., Minh, B.Q., and Vinh, L.S. (2018). Ufboot2: Improving the ultrafast bootstrap approximation. Mol. Biol. Evol. *35*, 518–522. https://doi.org/10.1093/molbev/msx281.

70. Guindon, S., Dufayard, J.F., Lefort, V., Anisimova, M., Hordijk, W., and Gascuel, O. (2010). New algorithms and methods to estimate maximum-likelihood phylogenies: Assessing the performance of phyml 3.0. Syst. Biol. *59*, 307–321. https://doi.org/10.1093/sysbio/syq010.

71. Smith, M.D., Wertheim, J.O., Weaver, S., Murrell, B., Scheffler, K., and Kosakovsky Pond, S.L. (2015). Less is more: An adaptive branch-site random effects model for efficient detection of episodic diversifying selection. Mol. Biol. Evol. *32*, 1342–1353. https://doi.org/10.1093/molbev/msv022.

72. Kosakovsky Pond, S.L., Poon, A.F.Y., Velazquez, R., Weaver, S., Hepler, N.L., Murrell, B., Shank, S.D., Magalis, B.R., Bouvier, D., Nekrutenko, A., et al. (2020). Hyphy 2.5-a customizable platform for evolutionary hypothesis testing using phylogenies. Mol. Biol. Evol. *37*, 295–299. https://doi.org/10.1093/molbev/msz197.

Please cite this article in press as: Akyuz et al., Evolutionary tuning of an auditory transduction channel, Current Biology (2026), https://doi.org/10.1016/j.cub.2026.02.059

STAR★METHODS

KEY RESOURCES TABLE

REAGENT or RESOURCE	SOURCE	IDENTIFIER
Bacterial and virus strains		
AAV9-PHP.B vectors encoding mouse Tmc1 variants	Boston Children's Hospital Viral Core	https://research.childrenshospital.org/resources/cores/viral-core/services
Chemicals, peptides, and recombinant proteins		
FM1-43 dye	Thermo Fisher Scientific	Cat# T35356
SCAS (4-Sulfonato calix[8]arene sodium salt)	VWR (Biotium)	Cat# 89139-432
Carbenicillin	VWR	Cat# 101414-060
HEPES	Sigma	Cat# #H3375
EGTA	Sigma-Aldrich	Cat# 97062-290
NaCl, KCl, $CaCl_2$ $MgCl_2$,CsCl	Sigma-Aldrich	N/A
MEM (1X) + GlutaMAX	Thermo Fisher Scientific	Cat# 41090-036
Fetal bovine serum (FBS)	Thermo Fisher Scientific	Cat# A5669701
HBSS	Thermo Fisher Scientific	Cat # 14025134
Recombinant DNA		
AAV-Tmc1ex1 plasmid (wild-type)	Previously published (Corey lab)	N/A
AAV-Tmc1ex1 plasmid (wild-type and mutant variants)	Genscript	N/A
Experimental models: Organisms/strains		
Tmc1Δ/Δ; Tmc2Δ/Δ mice (C57BL/6 background)	Andrew Griffith	Kawasima et al.[2]
CD-1 foster mothers	Charles River	CD1 (ICR)
Oligonucleotides		
hGH qPCR primers for viral titration	Boston Children's Hospital Viral Core	https://research.childrenshospital.org/resources/cores/viral-core/services
Deposited data		
Alignment and phylogenetic datasets	This study	Data S1; full datasets: https://gitlab.com/treyjscott/tmc
Software and algorithms		
AlphaFold3	AlphaFold Server	https://alphafoldserver.com/
PyMOL molecular graphics system	Schrödinger	v3.1.3
Clustal omega	EMBL-EBI	N/A
JalView	Jalview	v2.11.2.1
EMBOSS	EMBL-EBI	N/A
MAFFT	Katoh et al.[55]	v7.490
IQ-TREE	Nguyen et al.[56]	v2.3.0
ModelFinderUFBootSH-aLRT	IQ-TREE moduleIQ-TREE moduleIQ-TREE module	v2.3.0 v2.3.0v2.3.0
HyPhy	Pond et al.[57]	v2.5.62
HMMER	Eddy lab	v3.4
eggNOG-mapper	Hernandez-Plaza et al.[58]	V2.1.12
TM-align	Zhang Lab	https://zhanggroup.org/TM-align/
Clustvis	Metsalu et al.[59]	https://biit.cs.ut.ee/clustvis/
OrthoFinder	Emms and Kelly[60]	v2.5.5
ASTRAL-Pro3	Zhang et al.[61]	v1.22.3.6
GeneRax	Morel et al.[62]	V2.1.3
pal2nal	Suyama et al.[63]	V14

(*Continued on next page*)

Please cite this article in press as: Akyuz et al., Evolutionary tuning of an auditory transduction channel, Current Biology (2026), https://doi.org/10.1016/j.cub.2026.02.059

Continued

REAGENT or RESOURCE	SOURCE	IDENTIFIER
Clampfit	Molecular Devices	N/A
PCLAMP 10	Molecular Devices	N/A
Origin	OriginLab	N/A
Microsoft Excel	Microsoft	Version 16.106

EXPERIMENTAL MODEL AND STUDY PARTICIPANT DETAILS

Mouse strains

Tmc1$^{\Delta/\Delta}$Tmc2$^{\Delta/\Delta}$ mice on a C57BL/6 background[2] were used for all experiments. Neonatal pups were placed with CD-1 foster mothers (Charles River). ***Animal care and use***: All animals were housed and bred in the animal facility at Harvard Medical School and protocols were approved by the Institutional Animal Care and Use Committee (IACUC) at Harvard Medical School. ***Sex and age of animals***: Male and female pups were randomly chosen for the study. Injections were performed at postnatal day P1–P2, and tissues were collected at P4-P6 and cultured until use (P9-P18).

METHOD DETAILS

Consensus sequence generation

FASTA sequences of vertebrate TMC1-8 were downloaded from the Ensembl genome browser (release 113, http://useast.ensembl.org) and translated into protein sequences. Sequences for specific clades—including Jawless Fish (e.g., Lampreys), Cartilaginous Fish (e.g., Sharks, Rays), Bony / Ray-Finned Fish (e.g., Zebrafish), Lobe-Finned Fish (e.g., Coelacanth), Amphibians (e.g., Frogs), Reptiles and Birds (e.g., Lizards, Chickens), and Mammals (e.g., Humans, Mice)—were separately downloaded. Multiple sequence alignments (MSA) were performed with Clustal Omega[64] and visualized in JalView (version 2.11.2.1).[65] For each TMC subtype (TMC1-8), a consensus sequence was generated using EMBOSS by selecting the most frequent amino acid at each aligned position across extant sequences.

Structure prediction and similarity analysis

Full-length monomer sequences were used for all *Tmc* subtypes and species to generate individual protein models. For complex predictions, full-length mouse TMC1, TMIE, and CIB2 sequences were modeled together as dimers, reflecting the experimentally supported dimeric organization of the transduction complex. Structural models were generated using AlphaFold Server (AlphaFold3)[66] with default parameters. The top ranked model was used for all analyses; however, all five ranked models were examined to confirm consistency of the reported structural features. Predicted structures and per-residue confidence scores (pLDDT), exported as B-factors for visualization, were visualized in PyMOL version 3.1.3. (Schrödinger) using the standard coloring scheme. Experimentally determined structures of *C. elegans* TMC-1 (PDB ID: 7USW, 7USX) were used as references to assess conformational features and model TMIE interactions. To assess structural similarity across paralogs, predicted structures were compared and clustered using TM-align distance (TD) clustering.[26] For each pair, TM-scores normalized by both chain lengths were obtained, and the maximum TM-score was retained to construct the similarity matrix. The resulting matrix was visualized and hierarchically clustered using ClustVis.[59]

Evolution of TMC subfamilies

To understand the evolution of the TMC gene family, we downloaded proteomes of representative species from NCBI RefSeq (Data S1). We searched for TMC proteins in these proteomes with hmmscan in HMMER 3.4 with an E value of 10^{-9} using the TMC hmm profile from PFAM.[67] To confirm proteins that were found with hmmscan, we performed functional annotation with eggnog-mapper.[58] We also filtered sequences shorter than 300 amino acids. To understand the evolutionary relationships between TMCs, we inferred a maximum likelihood gene tree. We first aligned protein sequences with MAFFT v7.490 using the L-INS-I algorithm.[55] We found the best fitting model of sequence evolution using ModelFinder[68] with default parameters implemented in IQ-tree version 2.3.0[56] and used the best tree from 10 maximum likelihood tree estimates. To access node support, we performed 1000 ultrafast bootstraps[69] and 1000 bootstraps for the SH-like approximate likelihood ratio tests.[70] To characterize the pattern of duplication in TMC subfamilies, we reconciled subfamily gene trees with a species tree of echinoderms, a hemichordate, and chordates. To generate the species tree, we identified protein families across whole proteomes of our species with Orthofinder version 2.5.5 (using MAFFT alignments with -MSA flag).[60] We used the output gene trees from Orthofinder with at least 20 species represented to find the most parsimonious species tree using ASTRAL-Pro3 in the ASTER package.[61] This species tree was then reconciled with subfamily level gene trees with GeneRax[62] using models selected by ModelFinder in IQTree and the SPR strategy of reconciliation.

Please cite this article in press as: Akyuz et al., Evolutionary tuning of an auditory transduction channel, Current Biology (2026), https://doi.org/10.1016/j.cub.2026.02.059

Evolutionary selection analysis

To assess evolutionary pressures on TMC1 proteins, we generated alignments with MAFFT as described above. We filtered the alignment to use only positions with amino acids present in the mouse TMC1 protein using custom R scripts. We inferred an unrooted gene tree for TMC1 using IQ-tree with ModelFinder and selecting the best tree after ten runs. MAFFT protein alignments were used to generate codon alignments for selection analysis with pal2nal.[63] To detect episodic diversifying selection ($\omega > 1$) on specific branches of the TMC1 gene tree, Adaptive Branch-Site Random Effects Likelihood (aBSREL) analysis was performed using the HyPhy software package.[57,71] A similar aBSREL analysis was performed for TMC2, but without filtering the alignment according to mouse TMC1. To understand which sites may be driving patterns of selection across the TMC1 tree, we used the contrast Fixed Effects Likelihood method.[72] This method tests for differences in positive and negative selection between different branches. We tested for differences between (1) mammalian and background and (2) non-mammalian tetrapod and background (see Figure 3A).

AAV vector preparations

The AAV-Tmc1ex1 vector carries the mouse *Tmc1* coding sequence driven by a cytomegalovirus (CMV) promoter and followed by a human growth hormone (hGH) polyadenylation signal.[5] Point mutations were introduced in the coding sequence, and constructs were screened with an SmaI digest to check for ITR integrity before packaging into AAV9-PHP.B capsids by the Viral Core at Boston Children's Hospital. Genomic titers (measured with hGH primers) were between 2–10x10^{13} gc/ml. Vectors were aliquoted and stored at -80°C.

AAV virus injections

Tmc1$^{\Delta/\Delta}$*Tmc2*$^{\Delta/\Delta}$ C57BL/6 mice,[2] typically born ~ E20, were placed with CD1 foster mothers. Prior to injection at postnatal day P1-P2, mice were anesthetized using hypothermia. A post-auricular incision was made near the left ear with a cotton ball inserted to spread the tissue. Vector (1.2 μl) was injected through the round window membrane (RWM) using a Nanoliter 2000 Injector (World Precision Instruments) at a rate of 100 nl/min. Following the procedure, the surgical incision was closed with sutures. The pups were then put on a 37°C heating board to recover for 35 min and returned to their cages. Three animals of a litter were injected in a session, and we typically injected 2-3 litters per mutation. No blinding was applied during experimental procedures.

Cochlear dissection

At postnatal day P4 to P6, pups were euthanized by rapid decapitation, temporal bones were dissected, and the membranous labyrinth was isolated under a dissection microscope. Reissner's membrane was removed, and the tectorial membrane and stria vascularis were mechanically peeled away. Organs of Corti were excised and cultured in medium containing 98% MEM(1X) + GlutaMAX TM-I Minimum Essential Medium (41090-036 + Earl's salts) supplemented with 1% FBS, 10 mM HEPES and 0.05 mg/ml carbenicillin at 37°C in 5% CO_2. Each organ was pinned flat beneath a pair of thin glass fibers glued at one end with Sylgard to an 18-mm round glass coverslip. The organs were cultured until use (P9-18). The mid-basal section was used for patch-clamp recordings and the mid-apical section from the same explant was used to assess functional rescue by FM1-43 dye uptake.

FM1-43 dye uptake assay

Coverslips with adherent cochlear cultures were placed on a glass-bottomed chamber and rinsed three times with HBSS containing1.3 mM Ca^{2+}. Cultures were then incubated with 2 μM FM1-43 for one minute (unless otherwise indicated) followed by 10 μM SCAS (4-Sulfonato calix[8]arene, sodium salt) for two minutes and washed two additional times before imaging. Confocal imaging was performed on an Olympus FV1000 microscope with a 60X, 1.1-NA water-immersion objective. FM1-43 fluorescence (excitation at 488 nm with ~5-12 % intensity) was measured under identical acquisition settings across samples.

Electrophysiology

Hair cells were visualized using a Nikon Eclipse FNI microscope with 60X LWI objective and DIC optics, and transduction currents were recorded from inner hair cells with an Axopatch 200B patch clamp and a Digidata 1440 digitizer controlled by pCLAMP 10 software (Molecular Devices). The whole-cell voltage-clamp configuration was used for recordings. Currents were filtered at 5 kHz with a low-pass eight-pole Bessel filter. For hair bundle stimulation, custom glass probes were made and polished to a tip diameter of ~4 μm to match the shape of the inner hair cell bundles. The probe holder was moved by a piezo stack (Physik Instruments) driven by a custom high voltage driver amplifier. Probe displacements were calibrated using a stage micrometer under the same optical setup to ensure accurate step sizes. Each newly fabricated probe was first validated by recording wild-type TMC1 currents to confirm standard activation curves before proceeding with mutant recordings. Bundles were displaced for 80 ms with 15 step displacements ranging from -175 nm to +1050 nm at 88-nm increments. For recordings, 1.5 mm OD R-6 (8350) glass pipettes were pulled with a Narishige PC-10 puller. We patched inner hair cells that appeared morphologically intact and undamaged during the preparation, but we did not pre-select cells based on any reporter. In our previous work using the same AAV9-PHP.B delivery strategy, we established that ~90% of IHCs are transduced under these conditions,[25] making random patching highly likely to yield a transduced cell. In the *Tmc1/2*-null background, untransduced IHCs exhibit no mechanotransduction current; therefore, the presence of a MET current during recording served as a functional indicator of successful viral transduction. Patch pipettes were filled with an internal solution containing (in mM): 137 CsCl, 5 EGTA, 10 HEPES, 2.5 Na_2-ATP, 0.1 $CaCl_2$ and 3.5 $MgCl_2$, and adjusted to pH 7.4 with CsOH. The tissues were bathed in external solution containing (in mM): 137 NaCl, 5.8 KCl, 0.7 NaH_2PO_4, 10 HEPES, 1.3 $CaCl_2$, 0.9 $MgCl_2$,

Please cite this article in press as: Akyuz et al., Evolutionary tuning of an auditory transduction channel, Current Biology (2026), https://doi.org/10.1016/j.cub.2026.02.059

5.6 glucose, vitamins, and essential amino acids, and adjusted to pH 7.4 with NaOH. Cells were held at a -80 mV potential and a separate pipet flowed extracellular solution onto their apical surfaces. Sample sizes and statistics are reported in the figure panels and legends. Unless otherwise noted, data are mean ± SEM; n denotes cells.

QUANTIFICATION AND STATISTICAL ANALYSIS

Electrophysiological data were analyzed with Clampfit (Molecular Devices) and ORIGIN (OriginLab). For each cell, the average maximum current amplitudes as a function of probe displacement were plotted and fitted with a Boltzmann equation using ORIGIN as follows:

$$Y = \frac{A1 - A2}{1+\exp\left[\frac{(X - X_0)}{dx}\right]} + A2$$

where X is the bundle displacement, X_0 is the half-activation position, and dx is the slope factor that represents the mechanical sensitivity of the channel.

The data were normalized for each cell, such that A1 and A2 range from 0 to 1 to allow comparison across cells. For each TMC1 variant, X_0 values were reported as mean ± SEM of all cells (n=cells). Statistical comparisons between wild-type and mutant X_0 values were performed in Excel using two-tailed t-tests assuming unequal variance (Welch's correction). Statistical details, including sample sizes and exact p-values, are provided in the figure panels and legends. Results were considered significant at $p < 0.05$.

Energy calculations also followed from this analysis with:

$$\frac{\Delta G}{kT} = \frac{\Delta X_0}{dx},$$

where ΔX_0 is the shift in midpoint position relative to wild type and dx is the slope parameter derived from the activation-curve fits. For mutations that shifted the activation curve toward positive displacements and showed no significant change in slope (from wild-type TMC1 with dx= 149±13 nm), midpoint shifts in the 150-300 nm range correspond to ~1-2 kT changes in gating energy.

Activation curves from wild-type and mutant TMC1 aligned closely across cells (typically within ~50 nm), consistent with adaptation mechanisms that adjust channel activation to probe-defined bundle position. Because adaptation is incomplete (~80% compensation of static displacement), residual shifts in X_0 are interpreted as intrinsic changes in channel gating. Energetic estimates therefore likely represent lower bounds.